Supplementary Information (SI) for Nanoscale.


**Supporting Information**

Figure S1 shows the SEM images of the nano-spherical probe and the pyramidal probe, respectively. It can be seen that the diameter of the nano-spherical probe is about 500 nm, and the diameter of the pyramidal probe is about 10 nm.

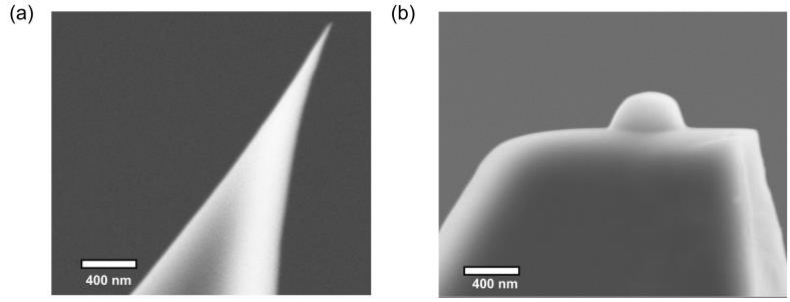


**Figure S1** (a) SEM image of the pyramidal probe, (b) SEM image of the nano-spherical probe.

The systematic simulations of the pressure distribution provide a more comprehensive understanding of the interaction between the pyramidal and nano-spherical probes with the 2D materials. Therefore, we have used the Hertz model to simulate the pressure distribution when the pyramidal and nano-spherical probes are in contact with the 2D materials[1]. The Hertz model provides a simplified yet accurate framework to model the contact mechanics in our study, where elastic deformation dominates, and adhesion forces are minimal. This allows us to effectively calculate the pressure distribution and contact radius using well-established elastic contact theory. Specifically, we have approximated the pyramidal probe as a 10 nm diameter sphere Hertz model and the nano-spherical probe as a 500 nm diameter sphere model.

In the Hertz model, the contact between a spherical probe and a flat plane can be described by the following formula, The contact radius, $a$, represents the size of the circular contact area formed when the spherical probe makes contact with the flat surface. The Hertz model provides the following formula for the contact radius:

$$a = \left(\frac{3FR}{4E^*}\right)^{\frac{1}{3}} \tag{1}$$

$F$ is the normal force applied to the probe, $R$ is the radius of the spherical probe, and $E^*$ is the effective elastic modulus of the two contacting bodies, which takes into account both the elasticity of the probe and the material it is contacting. The effective elastic modulus $E^*$ is calculated using Young's modulus and Poisson's ratios of the two materials involved (the probe and the plane surface). It is given by

$$\frac{1}{E^*} = \frac{1 - v_1^2}{E_1} + \frac{1 - v_2^2}{E_2} \tag{2}$$

$E_1$ and $E_2$ are the Young's modulus of the probe and the material, respectively. $v_1$ and $v_2$ are the Poisson's ratios of the probe and the material. The maximum contact pressure $P_{max}$ occurs at the center of the contact area and is given by

$$P_{max} = \frac{3F}{2\pi a^2} \tag{3}$$

$F$ is the normal applied force, $a$ is the contact radius calculated previously. The indentation depth, or deformation $\delta$ of the material due to the applied force can be calculated using the following equation

$$\delta = \left(\frac{9F^2}{16E^{*2}R}\right)^{\frac{1}{3}} \tag{4}$$

$F$ is the applied force, $R$ is the radius of the spherical probe, $E^*$ is the effective elastic modulus as previously defined. The Hertz model assumes that the stress is distributed within the contact area, and the stress distribution is not uniform. The pressure decreases as you move from the center of the contact area to its edge. The stress distribution follows a parabolic profile and is given by

$$\sigma(r) = \sigma_0\left(1 - \frac{r^2}{a^2}\right)^{\frac{1}{2}} \tag{5}$$

$\sigma_0$ is the maximum pressure (calculated above). $r$ is the radial distance from the center of the contact area. $a$ is the contact radius.

To calculate the maximum contact pressure, deformation, and stress distribution using the Hertz model for different spherical probe diameters (10 nm and 500 nm), the tip of the pyramidal probe is equivalent to a 10 nm diameter spherical probe. The specific probe diameter parameters and sample material parameters are defined. Radius $R_1 = 5$ nm for the 10 nm diameter probe, and $R_2 = 250$ nm for the 500 nm diameter probe.

Since this research doesn't focus on mechanical modeling, the author decided to simplify the process by using Young's modulus of the $SiO_2$ layer. Calculating the effective modulus for the whole structure would involve complicated modeling, considering the interactions and thickness of each layer, which is time-consuming and requires advanced knowledge. Also, because the thin $MoS_2$ and h-BN layers are attached to a much thicker $SiO_2$ substrate, their mechanical behavior is heavily influenced by the $SiO_2$ layer. So, using the Young's modulus of $SiO_2$ ($E_{SiO_2}$= 70 GPa, $v_{SiO_2}$= 0.17)[2, 3] is a practical and reasonable approximation, making the analysis simpler while still giving a good idea of the structure's overall mechanical properties.

Next, the composite Young's modulus for the silicon dioxide sample and the silicon probe ($E_{Si}$= 130 GPa, $v_{Si}$= 0.27)[4, 5] will be calculated with equation (2), $E^*$ = 47.61 GPa. Next, the contact radius $a$ the maximus contact pressure $P_{max}$ can be calculated by equation (1) and equation (3), in the case of 200 nN force applied by both the nano-spherical probe and the pyramidal probe. The contact radius and maximum contact pressure of the nano-spherical probe (D = 500 nm) and pyramidal probe (D = 10 nm) are respectively. The contact radius of nano-spherical probe $a_{(D\,=\,500\,nm)} = 9.24\,nm$, the maximum contact pressure $P_{\max\,(D\,=\,500\,nm)} = 1.12\,GPa$ contact radius of the pyramidal probe $a_{(D\,=\,10\,nm)} = 2.51\,nm$, the maximum contact pressure $P_{\max\,(D\,=\,10\,nm)} = 15.17\,GPa$. As the probe diameter decreases, the contact area becomes smaller, concentrating the applied force over a smaller region, which significantly increases the maximum contact pressure, which leads to more damage to the fragile surface. The deformation $\delta$ of the material can be calculated with equation (4), the $\delta_{(D=500\,nm)} = 0.58\,nm$, $\delta_{(D=10\,nm)} = 0.34\,nm$. Next, calculate the stress distribution curve according to Equation (5), as shown in Figure S2, where the maximum stress $P_{max}$ occurs at the center of the contact region $r = 0$, the stress decreases as the radial distance $r$ increases, and when, the stress drops to zero. In addition, we conducted COMSOL simulations where both the nano-spherical and pyramidal probes were modeled as silicon hemispheres with diameters of 500 nm and 10 nm, respectively, interacting

with a 280 nm silica sample. These simulation results are illustrated in Figures S2(b) and (c). The COMSOL results corroborate our calculations, showing that as the probe diameter decreases, the applied force is concentrated over a smaller area, significantly increasing the maximum contact pressure, and potentially causing greater damage to delicate surfaces.

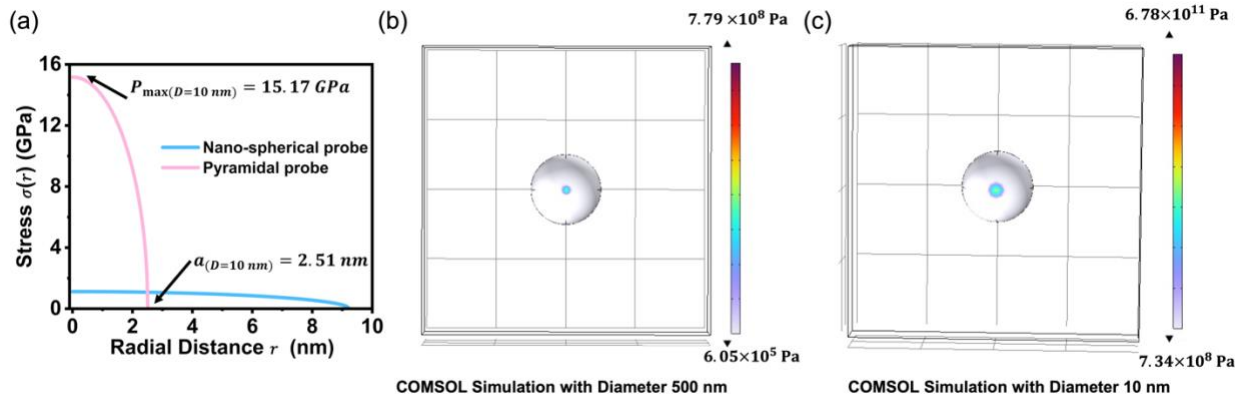


**Figure S2**(a) Pressure distribution of nano-spherical probe and pyramid probe under Hertzian model. (b) COMSOL simulation of the nano-spherical probe with a diameter 500 nm hemisphere. (c) COMSOL simulation with the pyramidal probe with a diameter 10 nm hemisphere.

Further experiments on $MoS_2$/hBN demonstrated the limited effectiveness of pyramidal probes, which only adequately cleaned smaller bubbles and caused damage in larger regions. Four distinct areas were tested: big, medium, and small bubble regions, and edge areas, using both nano-spherical and pyramidal probes. AFM images (Figure. S3 for nano-spherical probes and Figure. S4 for pyramidal probes) show that the nano-spherical probe effectively cleaned all areas without damage. In contrast, the pyramidal probe caused localized damage in medium-sized bubbles and was ineffective in larger bubbles, leading to material damage and warping at edges (Figure. S5 SEM images). These findings confirm the nano-spherical probe's superior non-destructive cleaning capability across various bubble sizes.

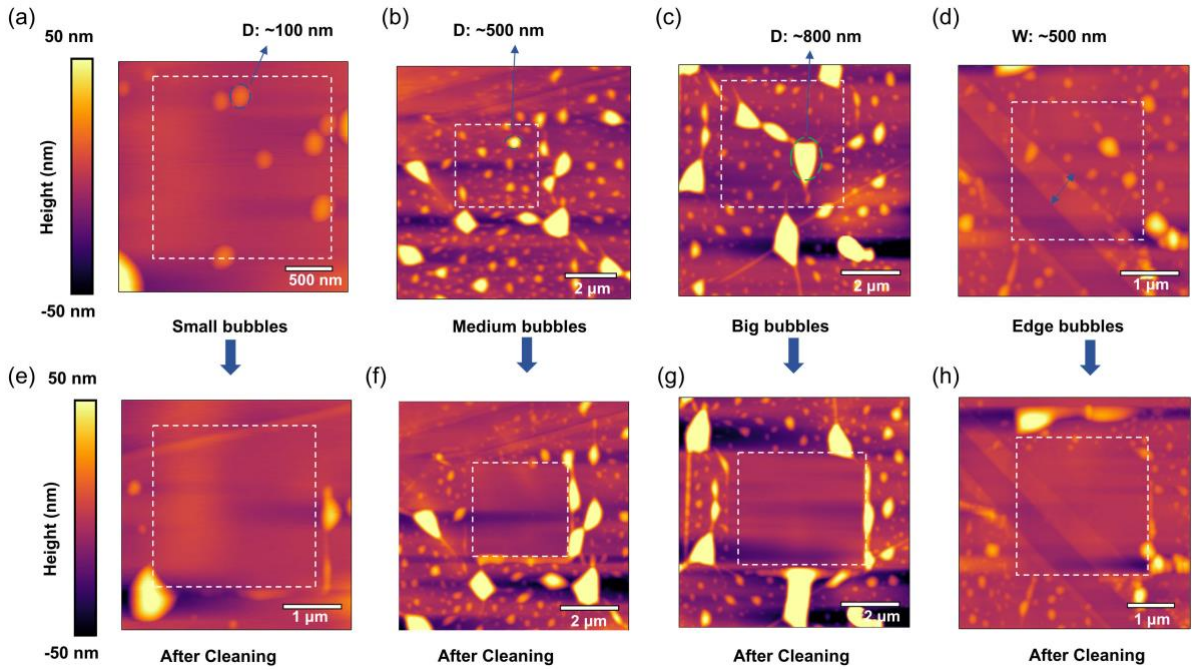


**Figure S3** depicts the AFM image before and after contact mode cleaning using the nano-spherical probe on the $MoS_2$/hBN substrate. Four distinct regions were identified for this study: areas with big bubbles defined as those exceeding 600 nm in diameter, medium bubbles defined from 300 to 599 nm, small bubbles ranging from 100 to 299 nm, and the edge region.

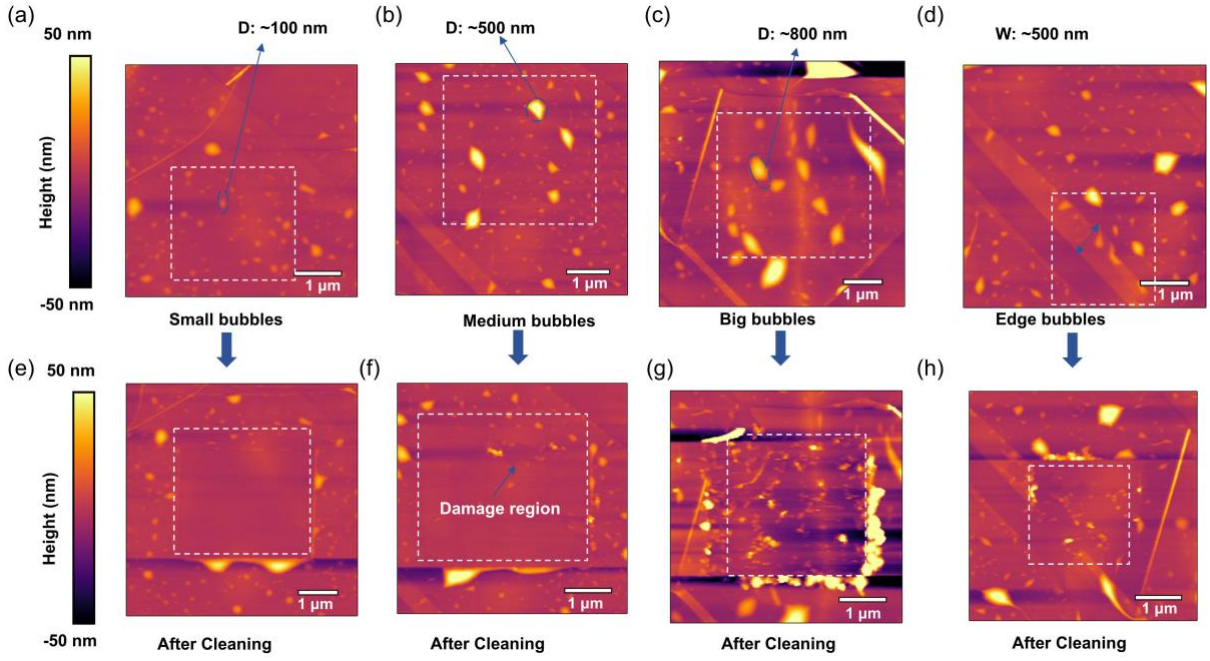

**Figure S4** depicts the AFM image before and after contact mode cleaning using the pyramidal probe on the $MoS_2$/hBN substrate. Four distinct regions were identified for this study: areas with big bubbles defined as those exceeding 600 nm in diameter, medium bubbles defined from 300 to 599 nm, small bubbles ranging from 100 to 299 nm, and the edge region.

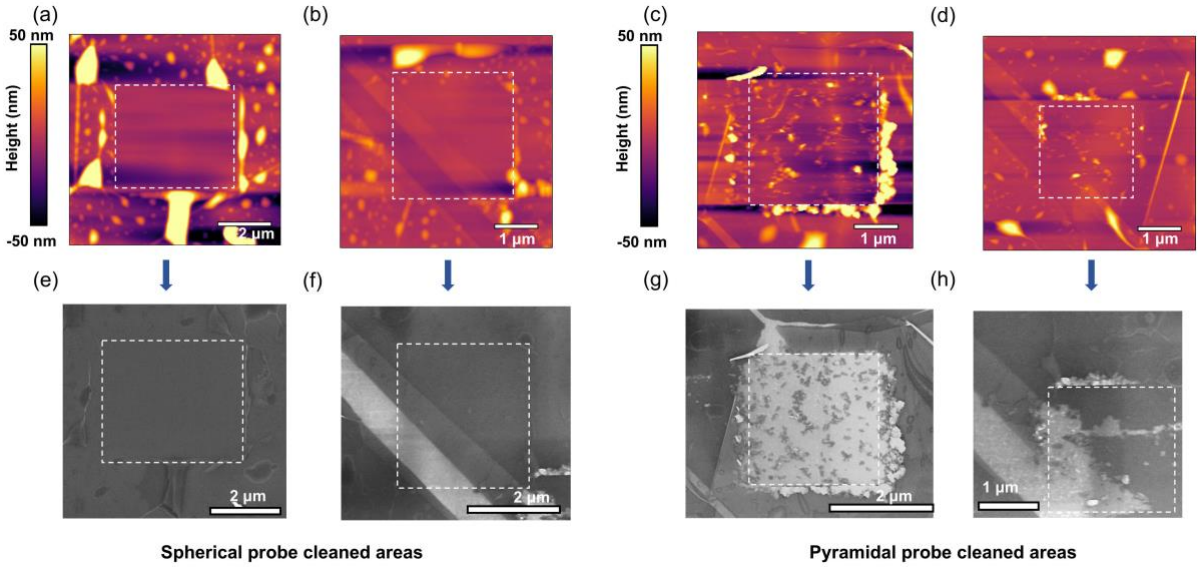


**Figure. S5**(a, b) and 3(e, f) show the AFM and SEM images, respectively, after cleaning with the nano-spherical probe. Fig. 3(c, d) and 3(g, h) show the AFM and SEM images, respectively, after cleaning with the pyramidal probe. The images clearly show that the pyramidal probe has caused damage to the material.

Figure S6 shows the AFM, SEM, and KPFM images following the application of a 300 nN force by a pyramidal probe aimed at removing residual bubbles. Figure S6(a) displays the AFM images of the regions cleaned by the nano-spherical probe, uncleaned regions, and the area cleaned by the pyramidal probe. Figure S6(b) presents the corresponding SEM images, and Figure S6(c) shows the KPFM images. The images on the right side of Figures S6(b) and (c) reveal inconsistencies in the surface morphology and electrical potential compared to other $MoS_2$ areas, indicative of crystal structure damage caused by the pyramidal probe during force application. This damage highlights the limitations of the pyramidal probe when cleaning larger bubbles or more complex interfaces, revealing structural instabilities induced by non-uniform force application on heterogeneous material surfaces.

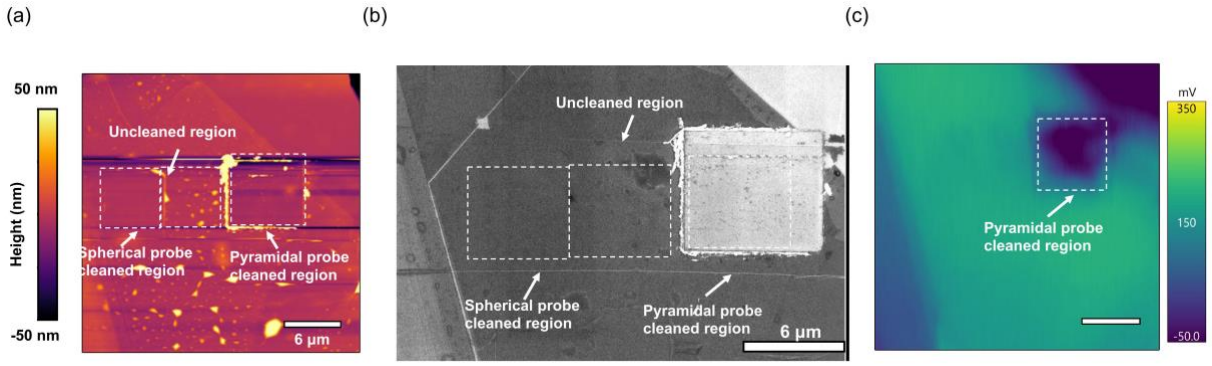


**Figure. S6** (a) shows AFM images of the nano-spherical probe cleaned region, uncleaned region, and region after a pyramidal probe was applied with 300 nN of force; (b) shows the corresponding SEM images; (c) shows the KPFM images.

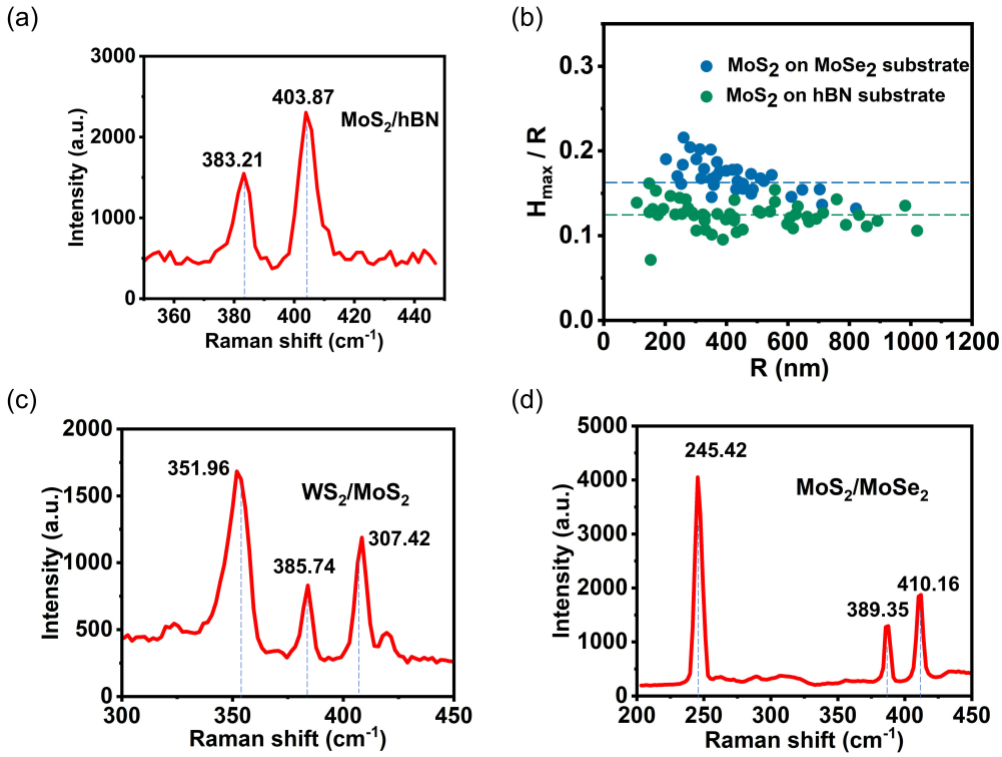


**Figure. S7** (a), (c), and (d) show the Raman spectra for $MoS_2$/hBN, $MoS_2$/$MoSe_2$/hBN, and $WS_2$/$MoS_2$ /hBN, respectively, while (b) shows the $H_{max}$/R graphs for $MoS_2$/hBN and $MoS_2$/$MoSe_2$/hBN.

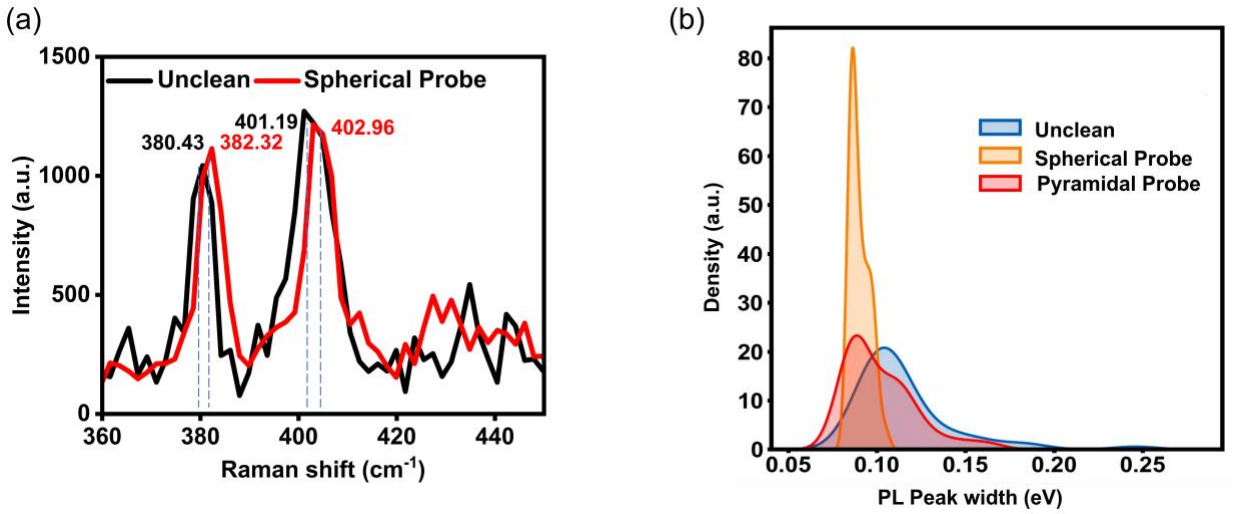


**Figure. S8** (a) The Raman data between the regions before and after nano-spherical probe cleaning, (b) The Kernel Density Estimation(KDE) fitting of the PL peak width of the uncleaned region, nano-spherical probe clean region and pyramidal probe clean region.

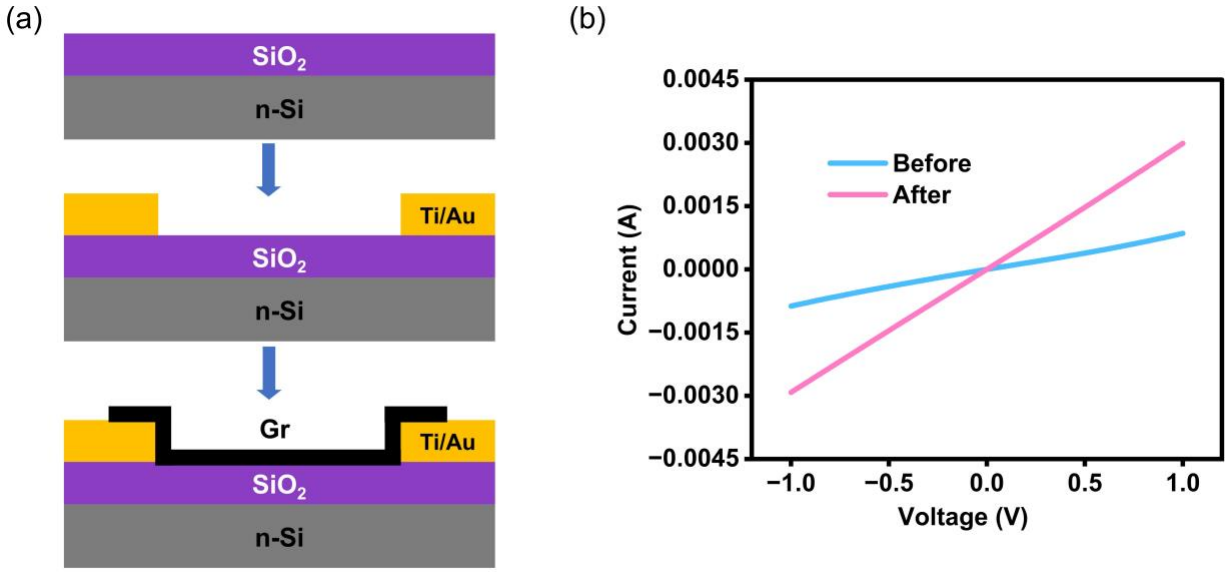


**Figure. S9**(a), the schematic shows the fabrication steps of the device, where a layer of Ti/Au is deposited on $SiO_2$/n-Si, followed by the addition of graphene Gr to complete the structure. (b) displays the I-V characteristics before and after nano-spherical probe treatment, with the pink curve ("After") showing improved current flow compared to the blue curve ("Before").

Under the conditions of a 2 μm scan range, 256 lines, and a 1 Hz scan rate, we conducted lateral force mode measurements on a $MoS_2$/hBN sample using both nano-spherical and pyramidal

probes. The measured deflection signals were approximately 10 mV for the nano-spherical probe and 20 mV for the pyramidal probe. it is shown in Figure S10. This indicates that, under identical conditions, the contact force between the pyramidal probe and the sample is greater than that of the nano-spherical probe. Consequently, the nano-spherical probe is less effective than the pyramidal probe in detecting surface sliding or frictional variations on the sample. Furthermore, no significant sliding was observed in the sample's topography.

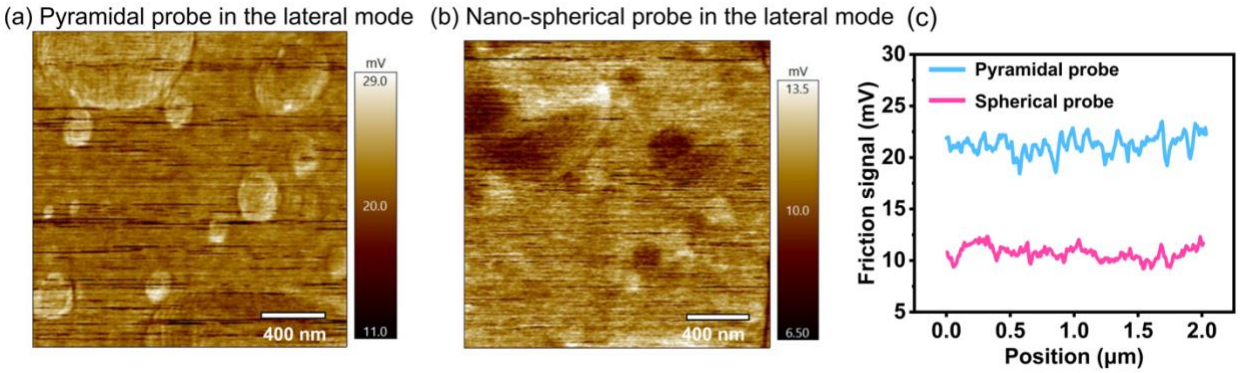


**Figure. S10** (a) The friction map obtained with a pyramidal probe. The range of the friction signal (20–29 mV) indicates a higher sensitivity to variations on the sample's surface. (b) presents the friction map with a nano-spherical probe. The signal range here (10–13.5 mV) is notably lower, producing a smoother map with less contrast in frictional variations. (c) The graph plots friction signals along the same scan distance for the pyramidal probe and nano-spherical probe.

References


1. Hertz, H., *The contact of elastic solids.* J Reine Angew, Math, 1881. **92**: p. 156-171.
2. Sharpe, W., et al., *Strain measurements of silicon dioxide microspecimens by digital imaging processing.* Experimental Mechanics, 2007. **47**: p. 649-658.
3. Ni, H., X. Li, and H. Gao, *Elastic modulus of amorphous SiO2 nanowires.* Applied Physics Letters, 2006. **88**(4).
4. Hopcroft, M.A., W.D. Nix, and T.W. Kenny, *What is the Young's Modulus of Silicon?* Journal of microelectromechanical systems, 2010. **19**(2): p. 229-238.
5. Vlassak, J. and W. Nix, *A new bulge test technique for the determination of Young's modulus and Poisson's ratio of thin films.* Journal of materials research, 1992. **7**(12): p. 3242-3249.